Nanoscale

PAPER

View Article Online
View Journal | View Issue

Cite this: *Nanoscale*, 2022, **14**, 13274

Magnetic particles for triggering insulin release in INS-1E cells subjected to a rotating magnetic field†

Svetlana Ponomareva,[a] Helene Joisten, [a,b] Taina François,[c] Cecile Naud,[a] Robert Morel, [a] Yanxia Hou,[c] Thomas Myers, [d] Isabelle Joumard,[a] Bernard Dieny *[a] and Marie Carriere *[c]

Diabetes is a major global health threat. Both academics and industry are striving to develop effective treatments for this disease. In this work, we present a new approach to induce insulin release from β-islet pancreatic cells (INS-1E) by mechanical stimulation. Two types of experiments were carried out. First, a local stimulation was performed by dispersing anisotropic magnetic particles within the cell medium, which settled down almost immediately on cell plasma membranes. Application of a low frequency magnetic field (up to 40 Hz) generated by a custom-made magnetic device resulted in oscillations of these particles, which then exerted a mechanical constraint on the cell plasma membranes. The second type of experiment consisted of a global stimulation, where cells were grown on magneto-elastic membranes composed of a biocompatible polymer with embedded magnetic particles. Upon application of a rotating magnetic field, magnetic particles within the membrane were attracted towards the field source, resulting in the membrane's vibrations being transmitted to the cells grown on it. In both experiments, the cell response to these mechanical stimulations caused by application of the variable magnetic field was quantified *via* the measurement of insulin release in the growth medium. We demonstrated that the mechanical action induced by the motion of magnetic particles or by membrane vibrations was an efficient stimulus for insulin granule secretion from β-cells. This opens a wide range of possible applications including the design of a system which triggers insulin secretion by β-islet pancreatic cells on demand.

Received 12th April 2022,
Accepted 27th July 2022

DOI: 10.1039/d2nr02009b

rsc.li/nanoscale

Introduction

Diabetes is a significant health challenge, with one in ten adults over the age of 18 being affected. It is the seventh leading cause of mortality, with 1.6 million deaths directly attributable to this disease in 2016.[1] The economic cost of diabetes is estimated to have risen from $245 billion in 2012 to $327 billion in 2017 in the United States.[1] Diabetes is a group of metabolic diseases characterized by a high sugar level in the blood. There are two types of diabetes, type 1 and type 2, type 2 diabetes being predominant with 90% of affected people. In type 1 diabetes, pancreatic beta cells fail to produce insulin and consequently the blood sugar level is not properly regulated. This condition could be fatal if insulin is not regularly administered to the patient. In type 2 diabetes, the body is resistant to insulin or insulin production is not sufficient. Although type 2 diabetes is known to be linked to excess body weight and lack of physical activity, the causes of type 1 diabetes are still unclear.

Effective treatment of diabetes requires continuous glucose monitoring (CGM) and the injection of an appropriate dose of insulin several times per day. The classical technique employed by people suffering from diabetes is to manually check the glucose level in their blood, and then to proceed with a sub-cutaneous injection of insulin if necessary. Recently, the concept of an artificial pancreas has emerged, also referred to as a "closed-loop system" or an "automated insulin delivery" system, or an "autonomous system for glycaemic control".[2] It is a system mimicking the function of a pancreas and composed of several devices that continuously monitor the blood glucose level, then determine the amount of insulin to inject, and deliver an appropriate dose of insulin.

Currently, research effort focuses on the use of live pancreatic β-cells to replace the GCM device and insulin infusion

[a]*Univ. Grenoble Alpes, CEA, CNRS, Grenoble INP, IRIG, SPINTEC, 38000 Grenoble, France. E-mail: bernard.dieny@cea.fr*
[b]*Univ. Grenoble Alpes, CEA, Leti, 38000 Grenoble, France*
[c]*Univ. Grenoble Alpes, CEA, CNRS, Grenoble INP, IRIG, SYMMES, 38000 Grenoble, France. E-mail: marie.carriere@cea.fr*
[d]*Platform Kinetics, Pegholme, Wharfebank Mills, Otley, LS21 3JP, UK*
† Electronic supplementary information (ESI) available. See DOI: https://doi.org/10.1039/d2nr02009b

pump, because these cells would both monitor blood glucose and release insulin when needed. Indeed, β-cells respond to an elevation of the glucose level in the bloodstream by triggering a well-orchestrated series of events, eventually leading to the exocytosis of insulin-containing granules out of the cell. Other chemical stimuli than glucose can trigger, stimulate or attenuate the release of insulin granules, including exposure to combinations of amino acids, fatty acids and some hormones.[3] In addition, some physical stresses have been proposed as inducers of insulin secretion, including applications of ultrasound[4] and mechanical stretch induced by cell swelling due to hypotonic stimulation.[5] These two physical stimuli induce insulin release *via* modulation of calcium influx into cells.

Live cells exhibit a strong response to mechanical stimulation. Accordingly, they can convert mechanical stimulus into biological activity, an effect known as mechanotransduction. Mechanical stimulation of live cells has been studied using various systems with a high degree of mechanical input including hydrostatic pressure, shear stress, substrate bending/distention, piezo-electric actuation, and magnetically induced actuation.[6–10] Several recent studies have dealt with their use in the field of cancer treatment to induce cancer cell death.[11–14]

In this context, we propose a new approach for efficient stimulation of insulin granule secretion from β-cells based on mechanotransduction. It relies on mechanical stimulation generated by magnetic microparticles (MPs) composed of $Fe_{20}Ni_{80}$ (so-called permalloy) subjected to a low frequency variable magnetic field (~20 Hz). Two experimental setups were designed, *i.e.*, magnetic particles were either applied directly to the cell surface or they were embedded within a magneto-elastic membrane (MEM) on which the cells were grown. The first setup results in a direct and strong stimulation of the cell membrane, while in the second setup the cells are stimulated by the soft movement of their support. In all these experiments, INS-1E cells, derived from pancreatic insulin secreting β-cells, were used. These cells present the main characteristics of pancreatic β-cells such as a relatively high insulin content and responsiveness to glucose within the physiological range.[15] We assumed that the mechanical action induced by the oscillations of magnetic particles or the vibrations of MEMs would efficiently stimulate insulin release, which was experimentally confirmed herein. The insulin stimulation protocol was optimized for its use under classical cell culture conditions while applying frequency- and amplitude-tunable magnetic fields. Our results suggest that it would be possible to design a system which triggers insulin secretion by β-islet pancreatic cells, on demand, by applying an external variable magnetic field.

Experimental

Fabrication of magnetic particles

Magnetic microparticles (MP) were produced by a top down approach exploiting standard microfabrication techniques: lithography, thin film deposition *etc*. The MP fabrication process is schematically shown in Fig. S1a† and includes the following steps: (1) spin coating of poly(methyl methacrylate) (PMMA) and ma-N 2403 resists (termed MAN in Fig. S1a†), (2) deep ultraviolet (DUV) lithography to create a template for particle arrays in ma-N 2403, (3) deposition of $Au/Fe_{20}Ni_{80}/Au$ layers by evaporation, (4) lift-off of the ma-N 2403 photoresist, and (5) lift-off of PMMA and collection of magnetic MPs.[16]

The first four steps result in the deposition of a regular square array with a pitch distance of 3 μm between $Fe_{20}Ni_{80}$ disks, which have a diameter of 1.3 μm and a height of up to 250 nm. SEM images confirm the lateral and vertical dimensions of MPs and the pitch distance (Fig. S1b–d†). This fabrication process allows the production of about 1 mg of 1.3 μm diameter $Au/Fe_{20}Ni_{80}/Au$ disks from a 4-inch wafer. The magnetic properties of these MPs have been described and modelled previously, as reported in our previous work.[17]

To decrease MP agglomeration after PMMA lift-off and to improve their biocompatibility, $Au/Fe_{20}Ni_{80}/Au$ MPs were functionalised with self-assembled monolayers of thiol molecules possessing amine terminal groups (1 mM of $HS\text{-}C_{11}\text{-}EG_6\text{-}NH_2$). For this, first, they were washed twice in ethanol. Second, ethanol was replaced by a thiol solution and the mixture was agitated for 2 hours. Third, MPs were washed twice in ethanol and then three times in glucose-free RPMI 1640. Finally, magnetic MPs were stored in a glucose-free medium at 4 °C for up to 3 weeks. The MP suspensions remained stable under this condition, they did not show any apparent agglomeration. For direct stimulation of INS-1E cells by deposition of magnetic particles on their surface, we prepared 10 nm/60 nm/10 nm $Au/Fe_{20}Ni_{80}/Au$ MPs using this procedure.

Fabrication of magneto-elastic membranes (MEMs)

For cell stimulation through the vibration of a magneto-elastic membrane (MEM) on which they are grown, thicker particles without Au coating were produced (200 nm of $Fe_{20}Ni_{80}$) (Fig. 1a). These MEMs consisted of magnetic MPs embedded in a polydimethylsiloxane (PDMS) layer. Their fabrication process included the four first steps described in Fig. S1a,† and then a 5 μm-thick layer of PDMS was spin-coated on the permalloy pattern. Then, the MEM was fixed on a PMMA tube, forming a well that could be filled with the cell culture medium.

In practice, first, a PMMA tube with external and internal diameters of 18 mm and 14 mm, respectively, and a height of 22 mm was glued with PDMS on top of the MEM (Fig. 1b). After 24–48 hours, the membrane was immersed in acetone for 10–15 min in order to dissolve the sacrificial layer of PMMA between the MEM and the silicon substrate (Fig. 1c and d). Once the membrane attached to the PMMA tube was released from the silicon substrate (Fig. 1e), it could be stored for months under ambient conditions. Then, the cells were grown in this well, adhering to the MEM. Using this procedure, the MEM was oriented so that the side on which the particles are covered by PDMS was positioned inside the well, so that MPs did not come into direct contact with cells. A schematic cross-sectional representation of this well, filled with the cell

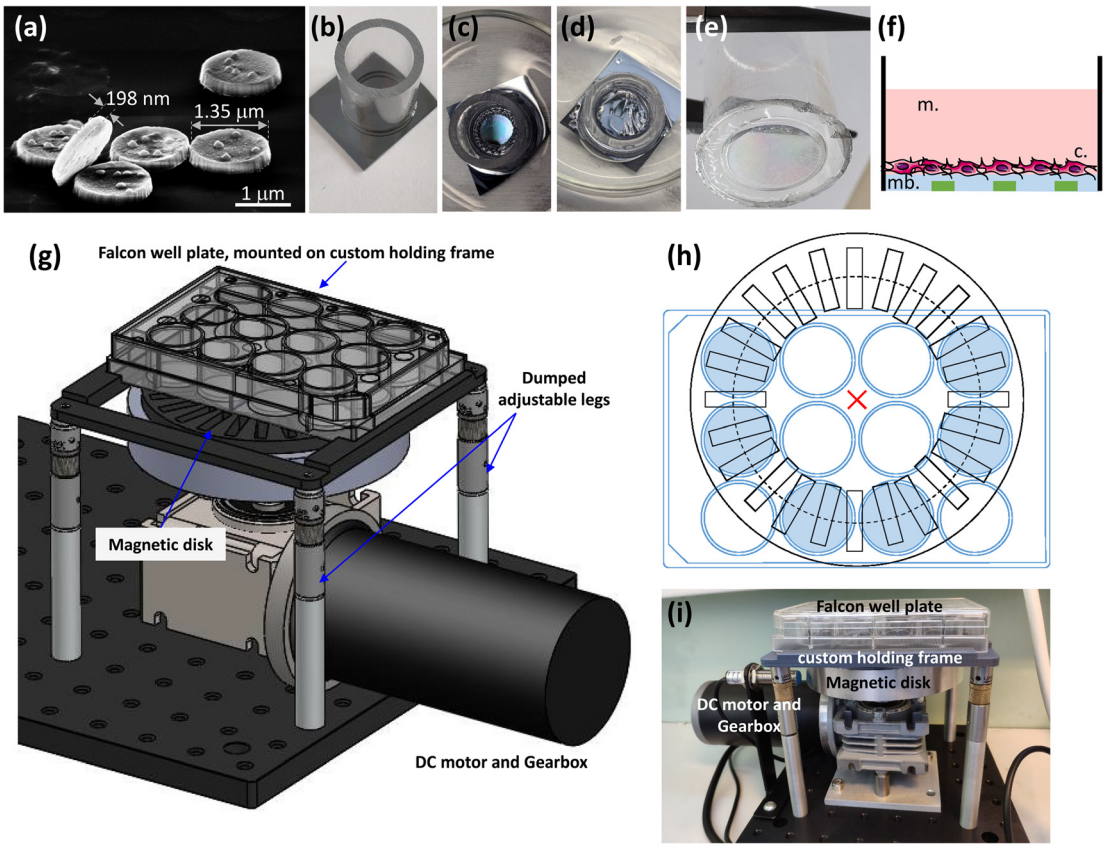

Fig. 1 Preparation of cell growth surfaces for magnetic actuation of FeNi particles. (a) SEM image of the $Fe_{20}Ni_{80}$ particles used for MEM fabrication; (b–e) fabrication of $Fe_{20}Ni_{80}$ particle-doped PDMS membranes: a PMMA tube is glued by PDMS to the membrane on a silicon substrate (b), then the sacrificial layer of PMMA between the substrate and the MEM is partially (c), and then fully (d) dissolved in acetone and the membrane attached to the PMMA substrate is released from the silicon substrate, forming a well in which cells can be grown (e). Schematic cross-sectional representation of the well formed by the PMMA tube (black) closed by the MEM; cell culture medium (m., pink), cells (c.), and the PDMS membrane (blue) with embedded 200 nm-thick $Fe_{20}Ni_{80}$ particles (green) (f). Magnetic field source device schematics (g and h): a spinning disk containing magnets is mounted on a speed controlled DC motor/gearbox that is mounted to an optical breadboard (g) and sits under a plastic frame holding the well plate (top view: h). The frame/plate is held above the disk on 4 adjustable pillars (g). Image of the system with a 12-well plate placed above spinning disk (i).

culture medium and with the cells growing on the MEM, is shown in Fig. 1f.

For better control of MEM elastic properties, two types of PDMS were used: Sylgard 184 silicon elastomer and Sylgard 527 dielectric gel (both from Dow Corning). Sylgard 184 was prepared by mixing a base and a cross linker in a 10 : 1 mass proportion (mixture 1), while Sylgard 527 was prepared by mixing part A and part B in a 1 : 1 mass proportion (mixture 2). Each mixture was manually stirred for 5 min and then degassed for 45 min. Variation in the ratio of mixture 1 and mixture 2 allows the Young's modulus to be tuned, starting from 5 kPa (corresponds to Sylgard 527) up to 1.72 MPa (corresponds to Sylgard 184).[18] For all experiments presented in this work, a 1 : 2 mass ratio between mixture 1 and mixture 2 was selected, leading to a Young's modulus of 460 kPa, so that the membrane could experience strong deformation without the risk of breaking.

Any type of PDMS or their mixture exhibit hydrophobic properties. So, before using such a membrane as a surface for growing cells, the MEM was activated by O_2 plasma for 3 min (gas composition: 75% of oxygen + 25% of argon; pressure: 0.6 mbar; and power: 20 W), in order to convert the hydrophobic PDMS surface to a hydrophilic surface[19] and therefore to improve cell adhesion. Then, they were sterilized by exposure to UV light for 20 min and finally they were washed in phosphate buffered saline (PBS). Alternative approaches, such as collagen or poly-L-lysine coating of PDMS did not show efficiency in promoting INS-1E cell adhesion.

A magnetic field source device for actuation of magnetic particles and MEMs

In order to apply the magnetic field, a specific magnetic device was designed and manufactured. It consists of a motorized spinning wheel (24 VDC 70 W DC motor with a 90 degree gearbox), carrying a set of 24 permanent magnets with alternating up and down polarity (Fig. 1g). A custom made frame allowed the positioning of a 12-well cell culture plate above the rotating magnets (Fig. 1h and i); its precise positioning was

tuned with adjustable legs (Fig. 1g). In the experiments consisting of actuating $Fe_{20}Ni_{80}$ particles directly on the surface of INS-1E cells, a 12-well plate containing the cells was directly attached on the fame. In the experiments involving MEMs glued on PMMA tubes, the PMMA tubes were fixed on a 3D printed plastic support allowing free membrane deformation when the magnetic field was applied. The magnets were 20 mm × 20 mm × 5 mm NdFeB, N42 grade, thin platelets with in-plane magnetization. The radius of the circle of magnets was designed so that six out of the twelve wells of the 12-well plate were above the magnet path (as represented in blue in Fig. 1h). Therefore, these six wells were exposed to the same alternating magnetic field. Since the field intensity above the magnets decreases with respect to the distance between the magnets and the plate, we could calibrate the field intensity by varying the *z*-position (height) of the plate. The magnetic field source device was stable and vibration-free at a rotation speed from 10 rpm to 300 rpm. A varying magnetic field up to 60 Hz could be obtained.

In order for the magnetic field source to be operated either on a bench or inside an incubator, the magnets were coated with epoxy to avoid oxidation. Moreover, the device controller was enclosed in a separate box, containing a power supply and a motor speed control board and a display, which could be operated from outside of the incubator.

Cell culture

INS-1E cells were grown from passage numbers 28 to 32 in RPMI 1640 medium (ThermoFisher Scientific) containing 10% fetal bovine serum, 10 mM HEPES, 1 mM sodium pyruvate, 2 mM L-glutamine, 100 units per mL penicillin, 100 μg mL^{-1} streptomycin and 50 μM 2-mercapto-ethanol. They were maintained at 37 °C and 5% CO_2 in a humidified atmosphere. The cells were passaged once a week using trypsin and seeded at a density of 6.7×10^4 cells per cm^2, *i.e.*, 5×10^6 cells in 75 cm^2 bottles containing 10 mL of medium. For all experiments, unless otherwise mentioned, the cells were seeded at 3×10^5 cells per well in 1 mL of medium in 12-well plates or at 1.2×10^5 cells per MEM in 0.4 mL of medium, corresponding to the same cell density as in 12-well plates. The cells were subjected to the treatments 48 h after seeding.

Insulin secretion stimulation protocol

The method for stimulation of insulin secretion was adapted from Merglen *et al.*[15] and is schematically represented in Fig. S2.† INS-1E cells were starved for 2 hours in glucose-free RPMI 1640 medium (ThermoFisher Scientific) containing 1% fetal bovine serum, 10 mM HEPES, 100 units per mL penicillin and 100 μg mL^{-1} streptomycin. Three wells contained only this starvation medium, while SAM-functionalized Au/$Fe_{20}Ni_{80}$/Au MPs were added in 12 wells (three wells per condition) at the following concentrations: 10 μg mL^{-1} (MP_10); 20 μg mL^{-1} (MP_20); and 50 μg mL^{-1} (MP_50). Next, the cells were washed twice in Krebs-Ringer-bicarbonate HEPES buffer (KRBH, 135 mM NaCl, 3.6 mM KCl, 5 mM $NaHCO_3$, 0.5 mM NaH_2PO_4, 0.5 mM $MgCl_2$, 1.5 mM $CaCl_2$, 10 mM HEPES, pH 7.4, and 0.1% (w/v) bovine serum albumin) and incubated for 30 min in KRBH. Due to their high sedimentation rate, the MPs were not eliminated during the washing steps. After this incubation period, the cells were exposed either to KRBH for another 30 min (CTL), or to 10–40 mM glucose prepared in KRBH for 30 min (positive control), or to the rotating magnetic field at 10, 20 or 40 Hz for 1, 5, 10 or 30 min.

Regarding the experiments on MEMs, the cells grown on PDMS membranes either with or without embedded magnetic particles were washed once in KRBH and then incubated in KRBH, either at 37 °C for 30 min without magnetic actuation, or in an incubator at 37 °C and 5% CO_2, on the magnetic device, while applying a rotating magnetic field of 10 Hz for 10 min.

The insulin concentration was quantified in the cell supernatants under all exposure conditions, after centrifugation, using an insulin ELISA assay (Mercodia) following the manufacturer's instructions except that the supernatants were allowed to react with the anti-insulin antibodies for 3 h rather than the recommended 1 h. Absorbance was measured at 450 nm for each well with calibrators and test samples, deposited in duplicate in the assay plate. The concentration of insulin in the test samples was obtained by data reduction from the calibration curve using cubic spline regression and taking into account the initial sample dilution. Finally, insulin concentrations were normalized compared to the level of insulin released in cells without any stimulation (CTL) (initially seeded at 3×10^5 cells per well in 1 mL of medium).

Cell viability and apoptosis assessment

For cell viability evaluation, cell metabolic activity was measured using the WST1 assay (Roche Applied Bioscience, France). The number of apoptotic cells was quantified using the CellEvent green assay (Thermo Fisher Scientific, France). In both assays, the cells were seeded at 3×10^5 cells per well in 12-well plates, and incubated for 48 h after seeding. For the WST1 assay, the cells were treated using the same protocol as for insulin secretion measurement. Positive controls were added to the experimental scheme, which consisted of cells exposed to 1% Triton X-100. At the end of the exposure period, exposure media were discarded and replaced by 500 μL of WST1 reagent diluted to the tenth in cell serum-free culture medium. The plates were incubated at 37 °C for 1 h, and then absorbance was measured at 450 nm using a Spectramax M2 spectrometer (Molecular Devices, Wokingham, UK). For the apoptosis assay, the cells were treated using the same protocol as for insulin secretion measurement, except that 1 μL of CellEvent green reagent was added in the first step of exposure, *i.e.*, during the 2 h starvation period. Staurosporine (0.3 μM) was used as a positive control. At the end of the exposure period, cell supernatants potentially containing some apoptotic cells were collected. The cells were then harvested using trypsin and added to the vials containing supernatants. These vials were centrifuged for 5 min at 200*g*. The cells were then fixed with 4% paraformaldehyde and analysed by flow cytometry using a FacsCalibur analyzer (BD Biosciences, Franklin

Lanes, NJ, USA) equipped with CXP software (Beckman Coulter Inc., Pasadena, CA, USA). Data were analysed using Flowing Software 2.5.1 (https://www.flowingsoftware.com/). The CellEvent reagent was also used for imaging apoptotic cells using the same protocol followed by imaging *via* epifluorescence microscopy using an Axiovert 200 microscope (Zeiss).

Electron microscopy

For INS-1E cell imaging by transmission electron microscopy (TEM) after exposure to $Fe_{20}Ni_{80}$ particles, the cells were rinsed with 0.1 M PHEM buffer (30 mM PIPES, 12.5 mM HEPES, 5 mM $MgCl_2$, and 1 mM EGTA, pH 7). They were then fixed in 4% paraformaldehyde (PFA), 0.4% glutaraldehyde and 0.2 M PHEM for 30 min at room temperature; and then for a further 30 min in a diluted solution composed of 1 volume of 4% PFA, 0.4% glutaraldehyde and 0.2 M PHEM and 1 volume of cell culture medium. The samples were then washed three times in 0.1 M PHEM and post-fixed for 1 h at room temperature in 1% osmium tetroxide (OsO_4), 1.5% potassium ferrocyanide prepared in 0.1 M PHEM buffer. After being washed three times with water, the samples were stained with 0.5% uranyl acetate prepared in 30% ethanol for 30 min at room temperature. The cells were then dehydrated in graded ethanol series and embedded in Epon resin. Ultrathin sections were prepared on a Leica UC7 ultra-microtome and collected on Formvar carbon-coated copper grids. Images were recorded on a Tecnai G2 Spirit BioTwin (FEI) microscope operating at 120 kV equipped with an ORIUS SC1000 CCD camera (Gatan).

Results and discussion

Triggering of insulin release from INS-1E cells with magnetic particles by application of a rotating magnetic field

To evaluate the effect of a rotating magnetic field on insulin secretion, first we assessed the responsiveness of INS-1E cells (Fig. 2a) to the increasing concentrations of glucose (Fig. 2b). The cells exposed for 30 min to glucose concentrations up to 20 mM resulted in a dose-dependent increase of insulin secretion with a plateau phase for higher glucose concentrations. These results are in agreement with previous studies.[11]

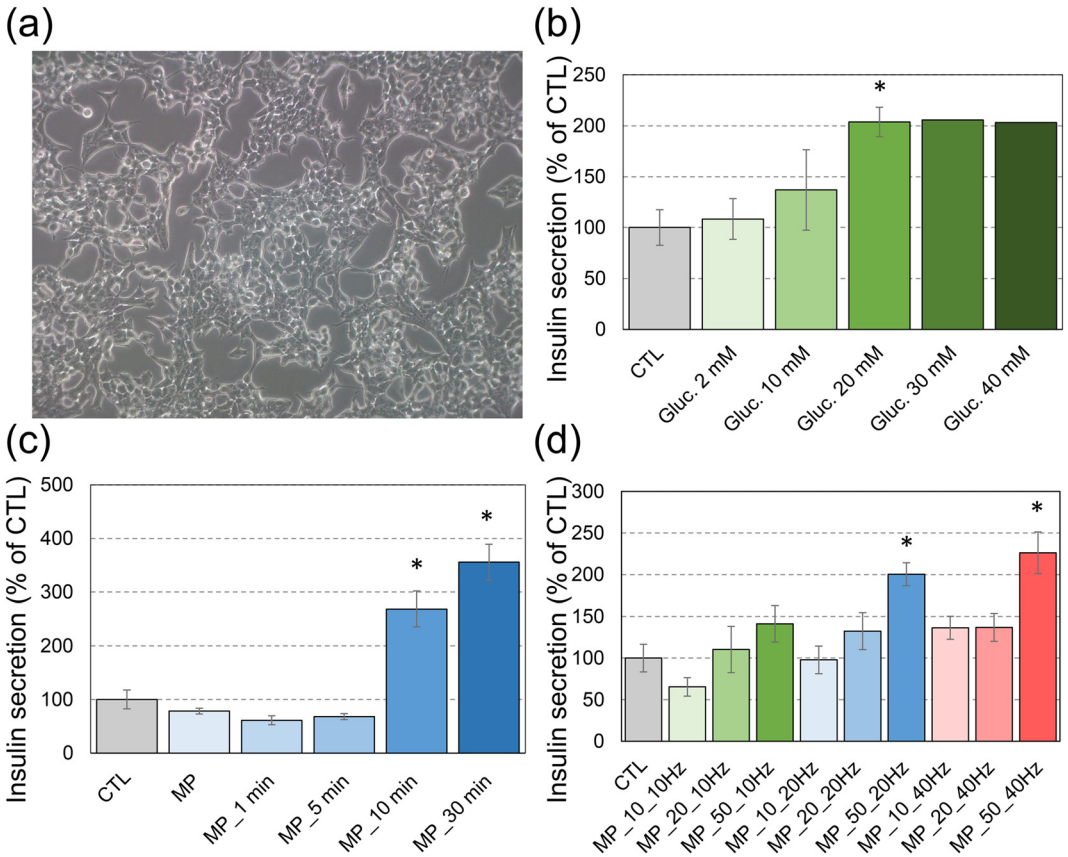

Fig. 2 Characterization of insulin secretion in INS-1E cells mechanically stimulated *via* application of magnetic particles on their plasma membranes and their actuation *via* a rotating magnetic field. (a) INS-1E cells before exposure to MPs and mechanical stimulation (magnification ×200); (b) stimulation of insulin secretion *via* exposure to 2, 10, 20, 30 or 40 mM of glucose for 30 min; (c) insulin secretion following exposure to 50 μg mL^{-1} MPs, and then application of a rotating magnetic field at 10 Hz for 1, 5, 10 or 30 min; and (d) insulin secretion following exposure to 10, 20 or 50 μg mL^{-1} MPs (MP_10, MP_20 and MP_50, respectively), and then application of a rotating magnetic field at 10 Hz, 20 Hz or 40 Hz for 10 min. Mean ± SEM of 3 experiments except for stimulation with 30 mM or 40 mM glucose (b), which was reproduced only twice. Statistical significance: *$p < 0.05$, exposed *vs.* CTL.

Once the responsiveness of cells to glucose was confirmed, magnetic MPs were introduced into the culture medium in order to apply mechanical stimulation on cell plasma membranes. First, we assessed the secretory response of cells to a fixed concentration of MPs (50 μg mL^{-1}) under a 10 Hz rotating magnetic field with respect to the duration of magnetic field application (Fig. 2c). When no rotating field was applied, the insulin secretion did not differ in cells exposed to magnetic particles, as compared to unexposed cells. When the rotating field was applied, insulin secretion remained the same as in control cells up to 5 min of mechanical stimulation. A significant increase in insulin release was observed for field exposure longer than 10 min. The insulin concentration became even larger for longer exposure to the field, up to 30 min (Fig. 2c). Therefore, a significantly increased insulin release was observed upon this long-term mechanical stimulation, which reached 2–3 fold the basal insulin release from control (unstimulated) INS-1E cells.

Then, the increasing concentrations of MPs were tested in order to determine the minimal concentration necessary to induce insulin secretion under the rotating magnetic field over a 10 min stimulation period (Fig. 2d). Both increasing MP concentrations and increasing frequency of the magnetic field enhanced the insulin secretion. The insulin concentration measured for cells exposed to 50 μg mL^{-1} of MPs and stimulated at 10 Hz was very close to the value obtained for cells with 10 μg mL^{-1} of MPs at 40 Hz.

To understand the interaction between the magnetic particles and INS-1E cells under the rotating magnetic field, optical images were recorded at different periods of time of mechanical stimulation (Fig. 3). During the first minutes of application of the magnetic field, the MPs appeared dispersed quite homogeneously on top of the cells (Fig. 3a). Their distribution remained almost unchanged after 5 min of magnetic treatment (Fig. 3b). However, longer application of the magnetic field for at least 10 min led some MPs to agglomerate as chains with a length up to 1–2 mm (Fig. 3c and d; black aggregates). Therefore, the observed significant increase of insulin release after 10 min of exposure to the rotating magnetic field might be associated with the formation of MP agglomerates. The vibration of these agglomerates under the rotating magnetic field should have a stronger mechanical effect on cell plasma membranes than the one caused by the vibration of single MPs. Insulin secretion upon mechanical stimulation of pancreatic β-cells has already been reported, using distinct mechanical stimulation techniques. First, apart from glucose stimulation, insulin secretion is known to be triggered by cell swelling, which is induced, for instance, when cells are exposed to a hypotonic osmotic stress.[20–23] Cell swelling leads to cell plasma membrane stretching, which triggers insulin secretion *via* the activation of volume-sensitive chloride (Cl^-) channels that in turn activate voltage-dependent Ca^{2+} channels (VDCCs).[20,21,24,25] This leads to a Ca^{2+} influx inside pancreatic β-cells, which is central to all insulin release mechanisms.[26] Other stretch-activated cation channels, and among them Piezo1, also play a role in insulin secretion in osmotically-induced cell swelling conditions *via* triggering Ca^{2+} influx inside the pancreatic β-cells.[5,27] Insulin secretion has also been reported to be induced by ultrasound stimulation, especially when cells are stimulated with 1 W cm^{-2} of ultrasound treatment from 400 kHz to 1 MHz.[28] Such stimulation also induces insulin secretion *via* generating a Ca^{2+} influx inside the β-cells.[4] In the present study, although it would need to be demonstrated, it is possible that Piezo1 mechanosensitive channels are implicated in the release of insulin observed after the magneto-mechanical stimulation. Indeed, these channels have been shown to be activated by distinct mechanical stimuli, all of them inducing plasma membrane deformations, including membrane stretch due to hypotonic treatment, shear stress, hydrostatic pressure, compression, ultrasound or piezoelectric microvibration.[27,29–33] This would allow the release of insulin, which could therefore contribute to the treatment of diabetes. Still, in contrast to all the other sources of the mechanical stimulation of pancreatic β-cells that have been described so far, the magneto-mechanical treatment proposed here can be finely tuned to be delivered to β-cells only, because $Fe_{20}Ni_{80}$ particles can be easily functionalized to promote targeted delivery. Indeed, they are covered with a thin Au layer, which has high affinity to thiolated ligands. Designing ligands that target specific pancreatic islet β-cell membrane receptors and present a thiolated moiety could be a simple way to deliver such particles specifically to these cells without affecting neighbouring cells.

Mechanical stimulation of human renal cancer cells *via* magnetic vibrations of the same type of particles was previously shown to induce cell death by apoptosis.[9] Therefore, both cell viability and the presence of apoptotic cells were monitored in the present system after treatment of INS-1E

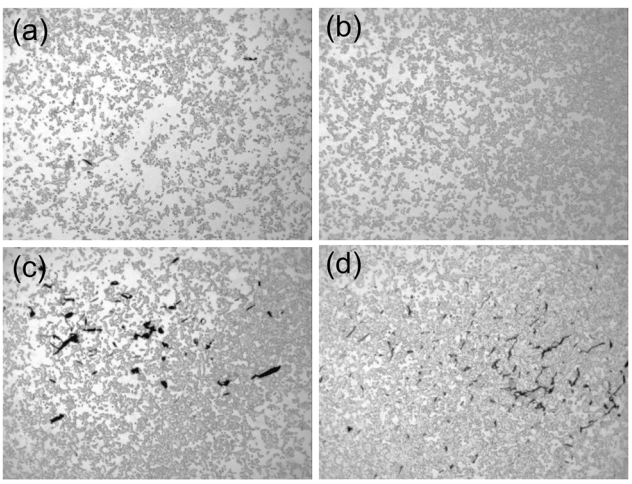

Fig. 3 Phase contrast microscopy images of INS-1E cells mechanically stimulated *via* application of magnetic particles on their plasma membranes and their actuation *via* a rotating magnetic field. Cells were exposed to 50 μg mL^{-1} MPs, and then a 10 Hz rotating magnetic field was applied for 1 min (a), 5 min (b), 10 min (c) or 30 min (d). Cells are visible as grey spheres while the black material is composed of MPs, self-organized as chaplets due to the application of the magnetic field. Magnification ×100.

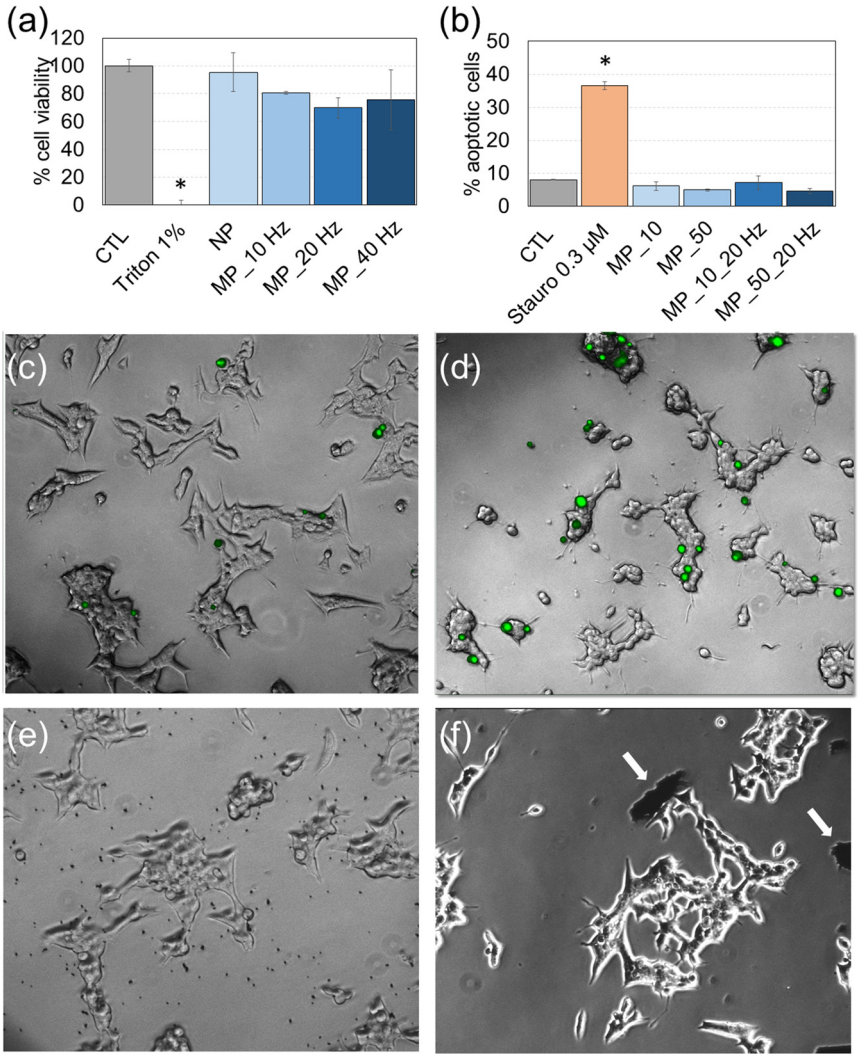

Fig. 4 Toxicity and apoptosis induced by MPs and mechanical stimulation. (a) WST-1 cytotoxicity assay on INS-1E cells exposed to 50 μg mL^{-1} of MPs (MP) or to 50 μg mL^{-1} of MPs combined to a 10, 20 or 40 Hz rotating magnetic field (MP_10 Hz, MP_20 Hz, and MP_40 Hz, respectively); triton 1% was used as a positive control. (b) INS-1E cells exposed to 10 or 50 μg mL^{-1} MPs (MP_10 and MP_50, respectively) or to 10 or 50 μg mL^{-1} MPs combined to a 20 Hz rotating magnetic field (MP_10_20 Hz and MP_50_20 Hz, respectively). Mean ± standard deviation of five replicates; statistical significance: *$p < 0.05$, exposed *vs.* CTL. (c) Control (unexposed) cells and cells exposed to 0.31 μM of staurosporine used as a positive control for apoptosis (d), or to 50 μg mL^{-1} MPs (e) or to 50 μg mL^{-1} MPs combined to a 20 Hz rotating magnetic field (f). In (c)–(f), grey images are phase contrast microscopy images and green cells are apoptotic cells, as probed by CellEvent green labelling and epifluorescence microscopy imaging. In (f), aggregates of MPs can be observed (white arrows).

cells with 10 or 50 μg mL^{-1} of MPs and application of a 20 Hz rotating magnetic field for 10 min (Fig. 4). No overt cell mortality and apoptosis were observed, whereas the respective positive controls, *i.e.*, triton 1% and staurosporine 0.3 μM showed high levels of cell mortality (Fig. 4a) and apoptosis (Fig. 4b). Fluorescence microscopy of apoptotic cells, *via* CellEvent green staining, confirmed the onset of apoptosis in positive control cells (*i.e.*, exposed to staurosporine, Fig. 4d), while only a few apoptotic cells were observed in control (unexposed) cells (Fig. 4c) or cells exposed to 50 μg mL^{-1} of MPs, either associated or not with a 20 Hz rotating magnetic field (Fig. 4e and f).

Interestingly, apoptosis induction and insulin secretion share a common mechanism, which is the elevation of the intracellular Ca^{2+} content. Moreover, the Piezo1 channel has been reported to trigger not only insulin secretion,[27] but also pancreatic cancer cell apoptosis when cells are stimulated *via* ultrasound,[34] with an implication of Ca^{2+} intracellular influx in both cases. Fine tuning of mechanical stimulation on pancreatic islet β-cells is thus highly necessary because depending on the power of the applied mechanical stimulus it would trigger either a beneficial outcome, *i.e.*, insulin secretion or cell death. Moreover, the efficiency of mechanical treatment used to induce insulin release would be highly dependent on the expression level of Piezo1 channels, which certainly depends on the cell type and shows inter-individual variation.

Finally, electron microscopy imaging confirmed that MPs interacted with cell plasma membranes (Fig. 5). Although no

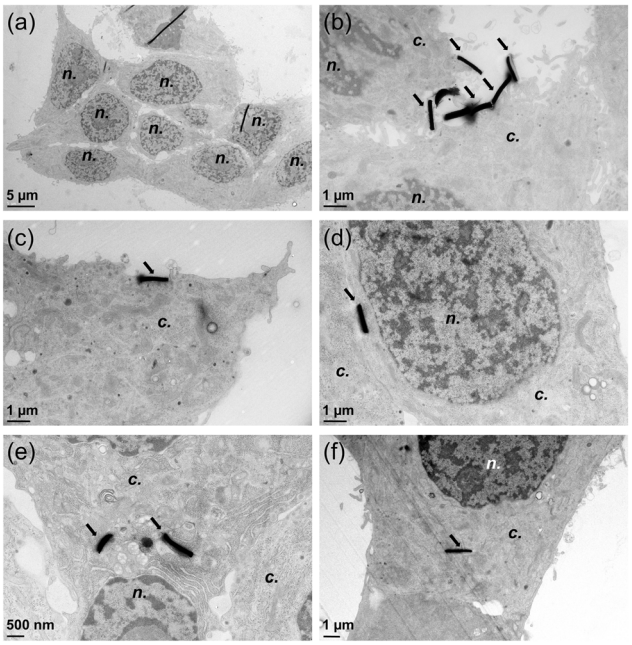

Fig. 5 Transmission electron microscopy images of INS-1E cells exposed to magnetic particles. Control cells (a), cells exposed to 50 μg mL^{-1} of MPs with no actuation (b) or to 50 μg mL^{-1} followed by actuation of the MPs *via* a magnetic field of 10 Hz (c), 20 Hz (d) or 40 Hz (e and f). Magnetic MPs are the dark materials indicated by arrows visible on cell membranes (b and c) or inside the cells (d–f); n.: cell nucleus; c.: cell cytoplasm.

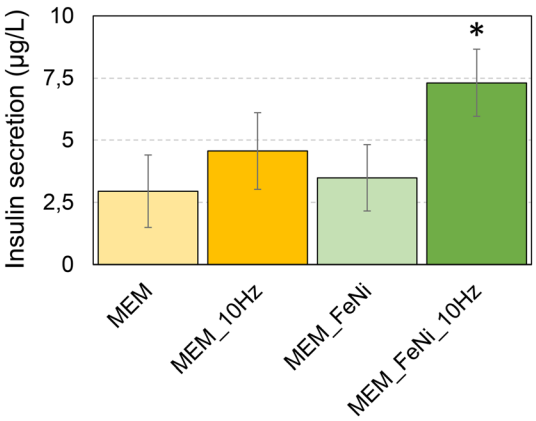

Fig. 6 Effect of a rotating magnetic field on insulin release from cells grown on MEMs. MEMs that do not contain magnetic particles, either not subjected to the rotating magnetic field (light yellow bar) or subjected to 10 min of a 10 Hz rotating magnetic field (orange bar). MEMs doped with $Fe_{20}Ni_{80}$ particles, either not actuated (light green bar) or actuated for 10 min *via* a 10 Hz magnetic field (dark green bar).

MPs were observed at the vicinity of control cells (not exposed to MPs) (Fig. 5a), some elongated-shaped electron-dense deposits were observed on the membranes of cells exposed to $Fe_{20}Ni_{80}$ MPs (Fig. 5b and c); their dimensions suggest that they are cross-sections of $Fe_{20}Ni_{80}$ MPs. After their actuation *via* the magnetic field, some MPs were also observed inside the cell cytoplasm (Fig. 5c–f). No membrane surrounded the MPs accumulated in the cell cytoplasm, suggesting that their internalization occurred *via* mechanical damage to the membrane rather than *via* endocytosis, which is considered to be the preferential internalization route for particles.[35]

Triggering of insulin release in cells grown on magneto-elastic membranes under the rotating magnetic field

Once the cell responsiveness to mechanical stimulation caused by magnetic MPs dispersed on the cell surface and exposed to the rotating magnetic field was confirmed, we investigated whether MEMs could be employed to trigger insulin release. Optical images of INS-1E cells 48 hours after seeding on the PDMS membrane treated or not with oxygen plasma are presented in Fig. S3.† Low adhesion and formation of the agglomerates of cells seeded on the hydrophobic surface of PDMS lead to cell death (Fig. S3a†), while the cells seeded on the O_2 plasma-treated hydrophilic surface show good adhesion and high viability (Fig. S3b and c†).

The effect of a rotating magnetic field on cells grown on MEMs was then studied *via* comparing insulin release from cells grown on MEMs that did not contain any magnetic particles to the insulin released from cells grown on magnetic particle-doped MEMs and actuated *via* a 10 Hz magnetic field for 10 min (Fig. 6). A significant increase of insulin release was clearly observed from cells grown on membranes subjected to the rotating magnetic field, and it was statistically significant only for MEMs containing $Fe_{20}Ni_{80}$ particles (Fig. 6a, MEM_FeNi_10 Hz). A slightly, but not statistically significant, increased insulin release was also observed from cells grown on membranes that did not contain magnetic particles, when subjected to the rotating magnetic field (Fig. 6a, MEM_10 Hz). This can be explained by possible membrane vibrations due to the air flux generated during the rotation of the wheel supporting the magnets. In our previous work,[17] we implemented an analytical model similar to the one described previously[36] to quantify the MEM profile and deformation at any point according to the applied pressure/force. This model was successfully validated by optical experiments in which the MEM was employed as a diffraction grating. The measured interference and diffraction patterns of flat and deformed membranes were in good agreement with simulation results. The MEM deformation due to the application of a magnetic field generated by our custom-made device was estimated to be several tens of micrometers which is of the order of the cell lateral dimensions and about 10 times larger than the MEM thickness.

Conclusions

In this article, we show that insulin release from INS-1E β-islet pancreatic cells can be induced *via* mechanical stimulation of the cells, either using vibration of magnetic particles deposited on their surface, or when growing the cells on a magneto-elastic membrane and stimulating its vibration. Magnetic par-

ticle vibration, directly on cell surfaces, is triggered by the application of a low frequency magnetic field from 10 to 40 Hz. Insulin release increases dramatically after 10 min of vibration, presumably due to the formation of MP chains. The MP concentration and frequency of the magnetic field play an important role in this process: an increase of one or the other parameters yields higher insulin release. Stimulation of cells *via* the vibration of a magnetoelastic membrane provides remote actuation of the membrane without direct contact between the cells and the MPs, thus lowering the risk of toxicity. It also gives the possibility to tune the membrane mechanical and optical properties (diameter, thickness, Young's modulus, transparency, *etc.*). Both approaches can be applied for different cell lines to study the mechanotransduction effect, opening a wide range of possible applications in biotechnology, in particular for tissue engineering and regenerative medicine. With respect to their suitability for the treatment of diabetes, the ability of the system to stimulate insulin secretion will need to be confirmed *in vivo* and the biocompatibility of the system should be carefully tested before a clear conclusion can be drawn.

Author contributions

SP and TF performed the biology experiments under the supervision of MC. SP and MC analyzed and curated the data. CN produced the magnetic particles, helped by RM and IJ. YH conceived the strategy to functionalize the magnetic particles; functionalization was carried out by SP and TF. TM developed and produced the device generating the rotating magnetic field. HJ, BD, RM, YH and MC acquired the project funding, conceptualized the study and developed the methodology. SP and MC wrote the initial draft, which was reviewed and edited by all authors.

Conflicts of interest

There are no conflicts to declare.

Acknowledgements

This work has received funding from the Horizon 2020 research and innovation programme of the EU under grant agreement no. 665440. The authors would like to thank F. Rivera for providing INS-1E cells, V. Collin-Faure for FACS analyses and C. Moriscot for electron microscopy sample preparation and imaging. S. Auffret is acknowledged for NiFe film deposition. This work used the EM facility and flow cytometry platform at the Grenoble Instruct-ERIC Center (ISBG; UMS 3518 CNRS CEA-UGA-EMBL) operated by C. Moriscot, with support from the French Infrastructure for Integrated Structural Biology (FRISBI; ANR-10-INSB-05-02) and GRAL, a project of the University Grenoble Alpes graduate school (Ecoles Universitaires de Recherche) CBH-EUR-GS (ANR-17-EURE-0003) within the Grenoble Partnership for Structural Biology. The IBS Electron Microscope facility is supported by the Auvergne Rhône-Alpes Region, the Fonds Feder, the Fondation pour la Recherche Médicale, and GIS-IBiSA.

References

1 W. H. Organization, *ISBN 978 92 4 156525 7 (NLM classification: WK 810)*, 2016.
2 N. Allen and A. Gupta, *Diagnostics*, 2019, **9**(1), 31–47.
3 Z. Fu, E. R. Gilbert and D. Liu, *Curr. Diabetes Rev.*, 2013, **9**, 25–53.
4 I. Suarez-Castellanos, T. Singh, B. Balteanu, D. C. Bhowmick, A. Jeremic and V. Zderic, *J. Ther. Ultrasound*, 2017, **5**, 30.
5 M. Takii, T. Ishikawa, H. Tsuda, K. Kanatani, T. Sunouchi, Y. Kaneko and K. Nakayama, *Am. J. Physiol.: Cell Physiol.*, 2006, **291**, C1405–C1411.
6 T. D. Brown, *J. Biomech.*, 2000, **33**, 3–14.
7 P. Campsie, P. G. Childs, S. N. Robertson, K. Cameron, J. Hough, M. Salmeron-Sanchez, P. M. Tsimbouri, P. Vichare, M. J. Dalby and S. Reid, *Sci. Rep.*, 2019, **9**, 12944.
8 Y. Sapir-Lekhovitser, M. Y. Rotenberg, J. Jopp, G. Friedman, B. Polyak and S. Cohen, *Nanoscale*, 2016, **8**, 3386–3399.
9 Q. Shi, H. Liu, D. D. Tang, Y. H. Li, X. J. Li and F. Xu, *NPG Asia Mater.*, 2019, **11**.
10 Y. Tai, A. Banerjee, R. Goodrich, L. Jin and J. Nam, *Polymers*, 2021, **13**.
11 D. H. Kim, E. A. Rozhkova, I. V. Ulasov, S. D. Bader, T. Rajh, M. S. Lesniak and V. Novosad, *Nat. Mater.*, 2010, **9**, 165–171.
12 S. Leulmi, X. Chauchet, M. Morcrette, G. Ortiz, H. Joisten, P. Sabon, T. Livache, Y. X. Hou, M. Carriere, S. Lequien and B. Dieny, *Nanoscale*, 2015, **7**, 15904–15914.
13 C. Naud, C. Thebault, M. Carriere, Y. X. Hou, R. Morel, F. Berger, B. Dieny and H. Joisten, *Nanoscale Adv.*, 2020, **2**, 3632–3655.
14 C. Thebault, M. Marmiesse, C. Naud, K. Pernet-Gallay, E. Billiet, H. Joisten, B. Dieny, M. Carriere, Y. Hou and R. Morel, *Nanoscale Adv.*, 2021, **3**, 6213–6222.
15 A. Merglen, S. Theander, B. Rubi, G. Chaffard, C. B. Wollheim and P. Maechler, *Endocrinology*, 2004, **145**, 667–678.
16 H. Joisten, T. Courcier, P. Balint, P. Sabon, J. Faure-Vincent, S. Auffret and B. Dieny, *Appl. Phys. Lett.*, 2010, **97**(25), 253112.
17 H. Joisten, A. Truong, S. Ponomareva, C. Naud, R. Morel, Y. Hou, I. Joumard, S. Auffret, P. Sabon and B. Dieny, *Nanoscale*, 2019, **11**, 10667–10683.
18 R. N. Palchesko, L. Zhang, Y. Sun and A. W. Feinberg, *PLoS One*, 2012, **7**, DOI: **10.1371/journal.pone.0051499**.
19 S. H. Tan, N. T. Nguyen, Y. C. Chua and T. G. Kang, *Biomicrofluidics*, 2010, **4**, DOI: **10.1063/1.3466882**.
20 L. Best, H. E. Miley and A. P. Yates, *Exp. Physiol.*, 1996, **81**, 927–933.

21 G. Drews, G. Zempel, P. Krippeit-Drews, S. Britsch, G. L. Busch, N. K. Kaba and F. Lang, *Biochim. Biophys. Acta*, 1998, **1370**, 8–16.
22 H. E. Miley, E. A. Sheader, P. D. Brown and L. Best, *J. Physiol.*, 1997, **504**(Pt 1), 191–198.
23 S. G. Straub, S. Daniel and G. W. Sharp, *Am. J. Physiol.: Endocrinol. Metab.*, 2002, **282**, E1070–E1076.
24 T. A. Kinard and L. S. Satin, *Diabetes*, 1995, **44**, 1461–1466.
25 E. A. Sheader, P. D. Brown and L. Best, *Mol. Cell. Endocrinol.*, 2001, **181**, 179–187.
26 M. Komatsu, M. Takei, H. Ishii and Y. Sato, *J. Diabetes Invest.*, 2013, **4**, 511–516.
27 V. Deivasikamani, S. Dhayalan, Y. Abudushalamu, R. Mughal, A. Visnagri, K. Cuthbertson, J. L. Scragg, T. S. Munsey, H. Viswambharan, K. Muraki, R. Foster, A. Sivaprasadarao, M. T. Kearney, D. J. Beech and P. Sukumar, *Sci. Rep.*, 2019, **9**, 16876.
28 I. Suarez-Castellanos, A. Jeremic, J. Cohen and V. Zderic, *Ultrasound Med. Biol.*, 2017, **43**, 1210–1222.
29 J. M. Hope, J. A. Dombroski, R. S. Pereles, M. Lopez-Cavestany, J. D. Greenlee, S. C. Schwager, C. A. Reinhart-King and M. R. King, *BMC Biol.*, 2022, **20**, 61.
30 Y. Fang, Q. Li, X. Li, G. H. Luo, S. J. Kuang, X. S. Luo, Q. Q. Li, H. Yang, Y. Liu, C. Y. Deng, Y. M. Xue, S. L. Wu and F. Rao, *Front. Cardiovasc. Med.*, 2022, **9**, 842885.
31 M. Luo, G. Cai, K. K. Y. Ho, K. Wen, Z. Tong, L. Deng and A. P. Liu, *BMC Mol. Cell Biol.*, 2022, **23**, 1.
32 A. Singh, A. Tijore, F. Margadant, C. Simpson, D. Chitkara, B. Chuan Low and M. Sheetz, *Bioeng. Transl. Med.*, 2021, **6**, e10233.
33 R. W. Wu, W. S. Lian, Y. S. Chen, J. Y. Ko, S. Y. Wang, H. Jahr and F. S. Wang, *Int. J. Mol. Sci.*, 2021, **22**(17), 9476.
34 Y. Song, J. Chen, C. Zhang, L. Xin, Q. Li, Y. Liu, C. Zhang, S. Li and P. Huang, *iScience*, 2022, **25**, 103733.
35 N. Oh and J. H. Park, *Int. J. Nanomed.*, 2014, **9**(Suppl 1), 51–63.
36 Y. Zhang, *Sci. China: Phys., Mech. Astron.*, 2016, **59**, 624602.